Charged hadron multiplicity fluctuations in Au+Au and Cu+Cu collisions from $\sqrt{s_{NN}} = 22.5$ to 200 GeV

A. Adare,[10] S. S. Adler,[5] S. Afanasiev,[24] C. Aidala,[11,39] N. N. Ajitanand,[52] Y. Akiba,[26,46,47] H. Al-Bataineh,[41] J. Alexander,[52] A. Al-Jamel,[41] K. Aoki,[30,46] L. Aphecetche,[54] R. Armendariz,[41] S. H. Aronson,[5] J. Asai,[47] E. T. Atomssa,[31] R. Averbeck,[53] T. C. Awes,[42] B. Azmoun,[5] V. Babintsev,[20] G. Baksay,[16] L. Baksay,[16] A. Baldisseri,[13] K. N. Barish,[6] P. D. Barnes,[33] B. Bassalleck,[40] S. Bathe,[6,36] S. Batsouli,[11,39,42] V. Baublis,[45] F. Bauer,[6] A. Bazilevsky,[5,47] S. Belikov,[5,20,23,*] R. Bennett,[53] Y. Berdnikov,[49] A. A. Bickley,[10] M. T. Bjorndal,[11,39] J. G. Boissevain,[33] H. Borel,[13] K. Boyle,[53] M. L. Brooks,[33] D. S. Brown,[41] N. Bruner,[40] D. Bucher,[36] H. Buesching,[5,36] V. Bumazhnov,[20] G. Bunce,[5,47] J. M. Burward-Hoy,[32,33] S. Butsyk,[33,53] X. Camard,[54] S. Campbell,[53] J.-S. Chai,[25] P. Chand,[4] B. S. Chang,[61] W. C. Chang,[2] J.-L. Charvet,[13] S. Chernichenko,[20] J. Chiba,[26] C. Y. Chi,[11,39] M. Chiu,[11,21,39] I. J. Choi,[61] R. K. Choudhury,[4] T. Chujo,[5,58] P. Chung,[52] A. Churyn,[20] V. Cianciolo,[42] C. R. Cleven,[18] Y. Cobigo,[13] B. A. Cole,[11,39] M. P. Comets,[43] P. Constantin,[23,33] M. Csanád,[15] T. Csörgő,[27] J. P. Cussonneau,[54] T. Dahms,[53] K. Das,[17] G. David,[5] F. Deák,[15] M. B. Deaton,[1] K. Dehmelt,[16] H. Delagrange,[54] A. Denisov,[20] D. d'Enterria,[11,39] A. Deshpande,[47,53] E. J. Desmond,[5] A. Devismes,[53] O. Dietzsch,[50] A. Dion,[53] M. Donadelli,[50] J. L. Drachenberg,[1] O. Drapier,[31] A. Drees,[53] A. K. Dubey,[60] A. Durum,[20] D. Dutta,[4] V. Dzhordzhadze,[6,55] Y. V. Efremenko,[42] J. Egdemir,[53] F. Ellinghaus,[10] W. S. Emam,[6] A. Enokizono,[19,32] H. En'yo,[46,47] B. Espagnon,[43] S. Esumi,[57] K. O. Eyser,[6] D. E. Fields,[40,47] C. Finck,[54] M. Finger Jr.,[7,24] M. Finger,[7,24] F. Fleuret,[31] S. L. Fokin,[29] B. Forestier,[34] B. D. Fox,[47] Z. Fraenkel,[60,*] J. E. Frantz,[11,39,53] A. Franz,[5] A. D. Frawley,[17] K. Fujiwara,[46] Y. Fukao,[30,46,47] S.-Y. Fung,[6] T. Fusayasu,[38] S. Gadrat,[34] I. Garishvili,[55] F. Gastineau,[54] M. Germain,[54] A. Glenn,[10,55] H. Gong,[53] M. Gonin,[31] J. Gosset,[13] Y. Goto,[46,47] R. Granier de Cassagnac,[31] N. Grau,[23] S. V. Greene,[58] M. Grosse Perdekamp,[21,47] T. Gunji,[9] H.-Å. Gustafsson,[35] T. Hachiya,[19,46] A. Hadj Henni,[54] C. Haegemann,[40] J. S. Haggerty,[5] M. N. Hagiwara,[1] H. Hamagaki,[9] R. Han,[44] A. G. Hansen,[33] H. Harada,[19] E. P. Hartouni,[32] K. Haruna,[19] M. Harvey,[5] E. Haslum,[35] K. Hasuko,[46] R. Hayano,[9] M. Heffner,[32] T. K. Hemmick,[53] T. Hester,[6] J. M. Heuser,[46] X. He,[18] P. Hidas,[27] H. Hiejima,[21] J. C. Hill,[23] R. Hobbs,[40] M. Hohlmann,[16] M. Holmes,[58] W. Holzmann,[52] K. Homma,[19] B. Hong,[28] A. Hoover,[41] T. Horaguchi,[46,47,56] D. Hornback,[55] M. G. Hur,[25] T. Ichihara,[46,47] V. V. Ikonnikov,[29] K. Imai,[30,46] M. Inaba,[57] Y. Inoue,[46,48] M. Inuzuka,[9] D. Isenhower,[1] L. Isenhower,[1] M. Ishihara,[46] T. Isobe,[9] M. Issah,[52] A. Isupov,[24] B. V. Jacak,[53,†] J. Jia,[11,39,53] J. Jin,[11,39] O. Jinnouchi,[46,47] B. M. Johnson,[5] S. C. Johnson,[32] K. S. Joo,[37] D. Jouan,[43] F. Kajihara,[9,46] S. Kametani,[9,59] N. Kamihara,[46,56] J. Kamin,[53] M. Kaneta,[47] J. H. Kang,[61] H. Kanou,[46,56] K. Katou,[59] T. Kawabata,[9] T. Kawagishi,[57] D. Kawall,[47] A. V. Kazantsev,[29] S. Kelly,[10,11,39] B. Khachaturov,[60] A. Khanzadeev,[45] J. Kikuchi,[59] D. H. Kim,[37] D. J. Kim,[61] E. Kim,[51] G.-B. Kim,[31] H. J. Kim,[61] Y.-S. Kim,[25] E. Kinney,[10] A. Kiss,[15] E. Kistenev,[5] A. Kiyomichi,[46] J. Klay,[32] C. Klein-Boesing,[36] H. Kobayashi,[47] L. Kochenda,[45] V. Kochetkov,[20] R. Kohara,[19] B. Komkov,[45] M. Konno,[57] D. Kotchetkov,[6] A. Kozlov,[60] A. Král,[12] A. Kravitz,[11,39] P. J. Kroon,[5] J. Kubart,[7,22] C. H. Kuberg,[1,*] G. J. Kunde,[33] N. Kurihara,[9] K. Kurita,[46,48] M. J. Kweon,[28] Y. Kwon,[55,61] G. S. Kyle,[41] R. Lacey,[52] Y.-S. Lai,[11,39] J. G. Lajoie,[23] A. Lebedev,[23,29] Y. Le Bornec,[43] S. Leckey,[53] D. M. Lee,[33] M. K. Lee,[61] T. Lee,[51] M. J. Leitch,[33] M. A. L. Leite,[50] B. Lenzi,[50] H. Lim,[51] T. Liška,[12] A. Litvinenko,[24] M. X. Liu,[33] X. Li,[8] X. H. Li,[6] B. Love,[58] D. Lynch,[5] C. F. Maguire,[58] Y. I. Makdisi,[5] A. Malakhov,[24] M. D. Malik,[40] V. I. Manko,[29] Y. Mao,[44,46] G. Martinez,[54] L. Mašek,[7,22] H. Masui,[57] F. Matathias,[11,39,53] T. Matsumoto,[9,59] M. C. McCain,[1,21] M. McCumber,[53] P. L. McGaughey,[33] Y. Miake,[57] P. Mikeš,[7,22] K. Miki,[57] T. E. Miller,[58] A. Milov,[53] S. Mioduszewski,[5] G. C. Mishra,[18] M. Mishra,[3] J. T. Mitchell,[5] M. Mitrovski,[52] A. K. Mohanty,[4] A. Morreale,[6] D. P. Morrison,[5] J. M. Moss,[33] T. V. Moukhanova,[29] D. Mukhopadhyay,[58,60] M. Muniruzzaman,[6] J. Murata,[46,48] S. Nagamiya,[26] Y. Nagata,[57] J. L. Nagle,[10,11,39] M. Naglis,[60] I. Nakagawa,[46,47] Y. Nakamiya,[19] T. Nakamura,[19] K. Nakano,[46,56] J. Newby,[32,55] M. Nguyen,[53] B. E. Norman,[33] A. S. Nyanin,[29] J. Nystrand,[35] E. O'Brien,[5] S. X. Oda,[9] C. A. Ogilvie,[23] H. Ohnishi,[46] I. D. Ojha,[3,58] H. Okada,[30,46] K. Okada,[46,47] M. Oka,[57] O. O. Omiwade,[1] A. Oskarsson,[35] I. Otterlund,[35] M. Ouchida,[19] K. Oyama,[9] K. Ozawa,[9] R. Pak,[5] D. Pal,[58,60] A. P. T. Palounek,[33] V. Pantuev,[53] V. Papavassiliou,[41] J. Park,[51] W. J. Park,[28] S. F. Pate,[41] H. Pei,[23] V. Penev,[24] J.-C. Peng,[21] H. Pereira,[13] V. Peresedov,[24] D. Yu. Peressounko,[29] A. Pierson,[40] C. Pinkenburg,[5] R. P. Pisani,[5] M. L. Purschke,[5] A. K. Purwar,[33,53] J. M. Qualls,[1] H. Qu,[18] J. Rak,[23,40] A. Rakotozafindrabe,[31] I. Ravinovich,[60] K. F. Read,[42,55] S. Rembeczki,[16] M. Reuter,[53] K. Reygers,[36] V. Riabov,[45] Y. Riabov,[45] G. Roche,[34] A. Romana,[31,*] M. Rosati,[23] S. S. E. Rosendahl,[35] P. Rosnet,[34] P. Rukoyatkin,[24] V. L. Rykov,[46] S. S. Ryu,[61] B. Sahlmueller,[36] N. Saito,[30,46,47] T. Sakaguchi,[5,9,59] S. Sakai,[57] H. Sakata,[19] V. Samsonov,[45] L. Sanfratello,[40] R. Santo,[36] H. D. Sato,[30,46] S. Sato,[5,26,57] S. Sawada,[26] Y. Schutz,[54] J. Seele,[10] R. Seidl,[21] V. Semenov,[20] R. Seto,[6] D. Sharma,[60] T. K. Shea,[5] I. Shein,[20] A. Shevel,[45,52] T.-A. Shibata,[46,56] K. Shigaki,[19] M. Shimomura,[57] T. Shohjoh,[57] K. Shoji,[30,46] A. Sickles,[53] C. L. Silva,[50] D. Silvermyr,[33,42] C. Silvestre,[13] K. S. Sim,[28] C. P. Singh,[3] V. Singh,[3] S. Skutnik,[23] M. Slunečka,[7,24] W. C. Smith,[1] A. Soldatov,[20] R. A. Soltz,[32] W. E. Sondheim,[33] S. P. Sorensen,[55] I. V. Sourikova,[5] F. Staley,[13] P. W. Stankus,[42] E. Stenlund,[35] M. Stepanov,[41] A. Ster,[27] S. P. Stoll,[5] T. Sugitate,[19] C. Suire,[43] J. P. Sullivan,[33] J. Sziklai,[27] T. Tabaru,[47] S. Takagi,[57] E. M. Takagui,[50] A. Taketani,[46,47] K. H. Tanaka,[26] Y. Tanaka,[38] K. Tanida,[46,47] M. J. Tannenbaum,[5] A. Taranenko,[52] P. Tarján,[14] T. L. Thomas,[40] M. Togawa,[30,46] A. Toia,[53] J. Tojo,[46] L. Tomášek,[22] H. Torii,[30,46,47] R. S. Towell,[1] V.-N. Tram,[31] I. Tserruya,[60] Y. Tsuchimoto,[19,46] S. K. Tuli,[3] H. Tydesjö,[35] N. Tyurin,[20] T. J. Uam,[37] C. Vale,[23] H. Valle,[58] H. W. van Hecke,[33] J. Velkovska,[5,58] M. Velkovsky,[53] R. Vertesi,[14] V. Veszprémi,[14] A. A. Vinogradov,[29] M. Virius,[12] M. A. Volkov,[29] V. Vrba,[22] E. Vznuzdaev,[45] M. Wagner,[30,46] D. Walker,[53] X. R. Wang,[18,41] Y. Watanabe,[46,47] J. Wessels,[36] S. N. White,[5] N. Willis,[43] D. Winter,[11,39] F. K. Wohn,[23] C. L. Woody,[5] M. Wysocki,[10] W. Xie,[6,47] Y. L. Yamaguchi,[59] A. Yanovich,[20] Z. Yasin,[6] J. Ying,[18]

S. Yokkaichi,[46,47] G. R. Young,[42] I. Younus,[40] I. E. Yushmanov,[29] W. A. Zajc,[11,39] O. Zaudtke,[36] C. Zhang,[11,39,42] S. Zhou,[8] J. Zimányi,[27,*] L. Zolin,[24] and X. Zong[23]
(PHENIX Collaboration)

[1]*Abilene Christian University, Abilene, Texas 79699, USA*
[2]*Institute of Physics, Academia Sinica, Taipei 11529, Taiwan*
[3]*Department of Physics, Banaras Hindu University, Varanasi 221005, India*
[4]*Bhabha Atomic Research Centre, Bombay 400 085, India*
[5]*Brookhaven National Laboratory, Upton, New York 11973-5000, USA*
[6]*University of California-Riverside, Riverside, California 92521, USA*
[7]*Charles University, Ovocný trh 5, Praha 1, CZ-11636, Prague, Czech Republic*
[8]*China Institute of Atomic Energy (CIAE), Beijing, People's Republic of China*
[9]*Center for Nuclear Study, Graduate School of Science, University of Tokyo, 7-3-1 Hongo, Bunkyo, Tokyo 113-0033, Japan*
[10]*University of Colorado, Boulder, Colorado 80309, USA*
[11]*Columbia University, New York, New York 10027, USA*
[12]*Czech Technical University, Zikova 4, CZ-16636, Prague 6, Czech Republic*
[13]*Dapnia, CEA Saclay, F-91191, Gif-sur-Yvette, France*
[14]*Debrecen University, H-4010 Debrecen, Egyetem tér 1, Hungary*
[15]*ELTE, Eötvös Loránd University, H-1117 Budapest, Pázmány P.s. 1/A, Hungary*
[16]*Florida Institute of Technology, Melbourne, Florida 32901, USA*
[17]*Florida State University, Tallahassee, Florida 32306, USA*
[18]*Georgia State University, Atlanta, Georgia 30303, USA*
[19]*Hiroshima University, Kagamiyama, Higashi-Hiroshima 739-8526, Japan*
[20]*IHEP Protvino, State Research Center of Russian Federation, Institute for High Energy Physics, Protvino RU-142281, Russia*
[21]*University of Illinois at Urbana-Champaign, Urbana, Illinois 61801, USA*
[22]*Institute of Physics, Academy of Sciences of the Czech Republic, Na Slovance 2, CZ-18221 Prague 8, Czech Republic*
[23]*Iowa State University, Ames, Iowa 50011, USA*
[24]*Joint Institute for Nuclear Research, RU-141980 Dubna, Moscow Region, Russia*
[25]*KAERI, Cyclotron Application Laboratory, Seoul, Korea*
[26]*KEK, High Energy Accelerator Research Organization, Tsukuba, Ibaraki 305-0801, Japan*
[27]*KFKI Research Institute for Particle and Nuclear Physics of the Hungarian Academy of Sciences (MTA KFKI RMKI), H-1525 Budapest 114, P. O. Box 49, Budapest, Hungary*
[28]*Korea University, Seoul 136-701, Korea*
[29]*Russian Research Center "Kurchatov Institute," Moscow, Russia*
[30]*Kyoto University, Kyoto 606-8502, Japan*
[31]*Laboratoire Leprince-Ringuet, Ecole Polytechnique, CNRS-IN2P3, Route de Saclay, F-91128, Palaiseau, France*
[32]*Lawrence Livermore National Laboratory, Livermore, California 94550, USA*
[33]*Los Alamos National Laboratory, Los Alamos, New Mexico 87545, USA*
[34]*LPC, Université Blaise Pascal, CNRS-IN2P3, Clermont-Fd, F-63177 Aubiere Cedex, France*
[35]*Department of Physics, Lund University, Box 118, SE-221 00 Lund, Sweden*
[36]*Institut für Kernphysik, University of Muenster, D-48149 Muenster, Germany*
[37]*Myongji University, Yongin, Kyonggido 449-728, Korea*
[38]*Nagasaki Institute of Applied Science, Nagasaki-shi, Nagasaki 851-0193, Japan*
[39]*Nevis Laboratories, Irvington, New York 10533, USA*
[40]*University of New Mexico, Albuquerque, New Mexico 87131, USA*
[41]*New Mexico State University, Las Cruces, New Mexico 88003, USA*
[42]*Oak Ridge National Laboratory, Oak Ridge, Tennessee 37831, USA*
[43]*IPN-Orsay, Universite Paris Sud, CNRS-IN2P3, BP1, F-91406, Orsay, France*
[44]*Peking University, Beijing, People's Republic of China*
[45]*PNPI, Petersburg Nuclear Physics Institute, Gatchina, Leningrad Region, RU-188300, Russia*
[46]*RIKEN, Institute of Physical and Chemical Research, Wako, Saitama 351-0198, Japan*
[47]*RIKEN BNL Research Center, Brookhaven National Laboratory, Upton, New York 11973-5000, USA*
[48]*Physics Department, Rikkyo University, 3-34-1 Nishi-Ikebukuro, Toshima, Tokyo 171-8501, Japan*
[49]*St. Petersburg State Polytechnic University, St. Petersburg, Russia*
[50]*Universidade de São Paulo, Instituto de Física, Caixa Postal 66318, São Paulo CEP05315-970, Brazil*
[51]*System Electronics Laboratory, Seoul National University, Seoul, Korea*
[52]*Chemistry Department, Stony Brook University, SUNY, Stony Brook, New York 11794, USA*
[53]*Department of Physics and Astronomy, Stony Brook University, SUNY, Stony Brook, New York 11794, USA*
[54]*SUBATECH (Ecole des Mines de Nantes, CNRS-IN2P3, Université de Nantes) BP 20722-44307, Nantes, France*

[55]*University of Tennessee, Knoxville, Tennessee 37996, USA*
[56]*Department of Physics, Tokyo Institute of Technology, Oh-okayama, Meguro, Tokyo 152-8551, Japan*
[57]*Institute of Physics, University of Tsukuba, Tsukuba, Ibaraki 305, Japan*
[58]*Vanderbilt University, Nashville, Tennessee 37235, USA*
[59]*Waseda University, Advanced Research Institute for Science and Engineering, 17 Kikui-cho, Shinjuku-ku, Tokyo 162-0044, Japan*
[60]*Weizmann Institute, Rehovot 76100, Israel*
[61]*Yonsei University, IPAP, Seoul 120-749, Korea*
(Received 11 May 2008; published 7 October 2008)

A comprehensive survey of event-by-event fluctuations of charged hadron multiplicity in relativistic heavy ions is presented. The survey covers Au+Au collisions at $\sqrt{s_{NN}} = 62.4$ and 200 GeV, and Cu+Cu collisions at $\sqrt{s_{NN}} = 22.5$, 62.4, and 200 GeV. Fluctuations are measured as a function of collision centrality, transverse momentum range, and charge sign. After correcting for nondynamical fluctuations due to fluctuations in the collision geometry within a centrality bin, the remaining dynamical fluctuations expressed as the variance normalized by the mean tend to decrease with increasing centrality. The dynamical fluctuations are consistent with or below the expectation from a superposition of participant nucleon-nucleon collisions based upon $p+p$ data, indicating that this dataset does not exhibit evidence of critical behavior in terms of the compressibility of the system. A comparison of the data with a model where hadrons are independently emitted from a number of hadron clusters suggests that the mean number of hadrons per cluster is small in heavy ion collisions.

DOI: 10.1103/PhysRevC.78.044902 PACS number(s): 25.75.Gz, 25.75.Nq, 21.65.Qr, 25.75.Ag

I. INTRODUCTION

Recent work with lattice gauge theory simulations has attempted to map out the phase diagram of quantum chromodynamics (QCD) in temperature and baryo-chemical potential (μ_B) using finite values of the up and down quark masses. The results of these studies indicate that the QCD phase diagram may contain a first-order transition line between the hadron gas phase and the strongly coupled quark-gluon plasma (sQGP) phase that terminates at a critical point [1]. This property is analogous to that observed in the phase diagram for many common liquids and other substances, including water. However, different model predictions and lattice calculations yield widely varying estimates of the location of the critical point on the QCD phase diagram [2]. Direct experimental observation of critical phenomena in heavy ion collisions would confirm the existence of the critical point, narrow down its location on the QCD phase diagram, and provide an important constraint for the QCD models.

The estimated value of energy densities achieved in heavy ion collisions at the BNL Relativistic Heavy Ion Collider (RHIC) exceeds the threshold for a phase transition from normal hadronic matter to partonic matter. Recent experimental evidence indicates that properties of the matter being produced include strong collective flow and large opacity to scattered quarks and gluons—the matter appears to behave much like a perfect fluid [3]. While measurements suggest the produced matter has properties that differ from normal nuclear matter, unambiguous evidence of the nature and location of any phase transition from normal nuclear matter has been elusive thus far. Described here is a search for direct evidence of a phase transition by measuring the fluctuations of the event-by-event multiplicities of produced charge particles in a variety of collision systems.

To illustrate how the measurement of charged particle multiplicity fluctuations can be sensitive to the presence of a phase transition, the isothermal compressibility of the system can be considered [4]. The isothermal compressibility is defined as

$$k_T = -1/V\,(\delta V/\delta P)_T\,, \tag{1}$$

where V is the volume, T is the temperature, and P is the pressure of the system. To relate the compressibility to measurements of multiplicity fluctuations, we assume that relativistic nucleus-nucleus collisions can be described as a thermal system in the grand canonical ensemble (GCE) [5]. The GCE can be applied to the case of measurements near midrapidity, since energy and conserved quantum numbers in this region can be exchanged with the rest of the system, which serves as a heat bath [6]. Detailed studies of multiplicity fluctuations in the canonical and microcanonical ensembles with the application of conservation laws can be found elsewhere [7,8]. In the GCE, the isothermal compressibility is directly related to the variance of the particle multiplicity as follows:

$$\langle (N - \langle N\rangle)^2\rangle = \mathrm{var}(N) = \frac{k_B T \langle N\rangle^2}{V} k_T, \tag{2}$$

where N is the particle multiplicity, $\langle N\rangle = \mu_N$ is the mean multiplicity, and k_B is the Boltzmann constant [9]. Here, multiplicity fluctuation measurements are presented in terms of the scaled variance, ω_N:

$$\omega_N = \frac{\mathrm{var}(N)}{\mu_N} = k_B T \frac{\mu_N}{V} k_T. \tag{3}$$

In a continuous, or second-order, phase transition, the compressibility diverges to an infinite value at the critical point.

*Deceased
†PHENIX spokesperson: jacak@skipper.physics.sunysb.edu

Near the critical point, this divergence is described by a power law in the variable $\epsilon = (T - T_C)/T_C$, where T_C is the critical temperature. Hence, the relationship between multiplicity fluctuations and the compressibility can be exploited to search for a clear signature of critical behavior by looking for the expected power law scaling of the compressibility,

$$k_T \propto \left(\frac{T - T_C}{T_C}\right)^{-\gamma} \propto \epsilon^{-\gamma}, \tag{4}$$

where γ is the critical exponent for isothermal compressibility [9]. If the QCD phase diagram contains a critical point, systems with a low value of baryo-chemical potential (μ_B) could pass through the cross-over region and undergo a continuous phase transition [2]. Recent estimates [10,11] of the behavior of the quark number susceptibility χ_q, which is proportional to the value of the isothermal compressibility of the system, predict that its value will increase by at least an order of magnitude close to the QCD critical point. Given that the scaled variance is proportional to k_T, measurements of charged particle multiplicity are expected to be a sensitive probe for critical behavior. In addition, within a scenario where droplets of QGP are formed during a first-order phase transition, the scaled variance of the multiplicity could increase by a factor of 10–100 [12].

Experimentally, a search for critical behavior is facilitated by the rich and varied dataset provided by RHIC. It is expected that the trajectory of the colliding system in the QCD phase diagram can be modified by varying the colliding energy [2]. If the system approaches close enough to the critical line for a long enough time period, then critical phenomena could be readily apparent through the measurement of multiplicity fluctuations [13]. It may also be possible to determine the critical exponents of the system. Nature tends to group materials into universality classes whereby all materials in the same universality class share identical values for their set of critical exponents. Although beyond the scope of this analysis, observation of critical behavior in heavy ion collisions and the subsequent measurement of the critical exponents could determine the universality class in which QCD is grouped, providing essential constraints for the models.

Charged particle multiplicity fluctuations have been measured in elementary collisions over a large range of collision energies [14–20]. Initial measurements of multiplicity fluctuations in minimum-bias O+Cu collisions at $\sqrt{s_{NN}} = 4.86$ GeV were made by BNL Experiment E802 [21], minimum-bias O+Au collisions at $\sqrt{s_{NN}} = 17.3$ GeV by CERN Experiment WA80 [22], and minimum-bias S+S, O+Au, and S+Au collisions at $\sqrt{s_{NN}} = 17.3$ GeV by CERN Experiment NA35 [23]. Recently, larger datasets have enabled the measurement of the centrality dependence of multiplicity fluctuations in Pb+Pb collisions at $\sqrt{s_{NN}} = 17.3$ GeV by CERN Experiment WA98 [24] and in Pb+Pb, C+C, and Si+Si collisions at $\sqrt{s_{NN}} = 17.3$ GeV by CERN Experiment NA49 [25]. The PHENIX Experiment at RHIC has performed an analysis of density correlations in longitudinal space with a differential analysis of charged particle multiplicity fluctuations in 200 GeV Au+Au collisions over the entire transverse momentum range [26]. Thus far, the fluctuation measurements in heavy ion collisions do not indicate significant signs of a phase transition. However, the full range of collision energies and species accessible by RHIC are yet to be explored.

Presented here is a comprehensive survey of multiplicity fluctuations of charged hadrons measured by the PHENIX Experiment at RHIC. The survey will cover the following collision systems: $\sqrt{s_{NN}} = 200$ GeV Au+Au, 62.4 GeV Au+Au, 200 GeV Cu+Cu, 62.4 GeV Cu+Cu, and 22.5 GeV Cu+Cu with comparisons to $\sqrt{s} = 200$ GeV $p+p$ collisions, which serve as a baseline measurement. The Au+Au data were taken during RHIC Run-4 (2004), the Cu+Cu data were taken during RHIC Run-5 (2005), and the $p+p$ data were taken during RHIC Run-3 (2003). Multiplicity fluctuations for each collision system with the exception of $p+p$ will also be presented as a function of centrality to help select the system volume. Multiplicity fluctuations will also be presented as a function of transverse momentum range and charge sign.

This paper is organized as follows: Sec. II will discuss the experimental apparatus and details; Sec. III will discuss the methods applied for the measurement of multiplicity fluctuations and the removal of nondynamical fluctuations due to fluctuations of the collision geometry within a centrality bin; Sec. IV will present the results and compare them to those of other models. Sec. V will present a discussion and summary of the results.

II. EXPERIMENTAL SETUP

The PHENIX detector consists of two central spectrometer arms designed for charged particle tracking, designated east and west, and two muon spectrometers designed for muon tracking and identification, designated north and south. The muon spectrometers are not used in this analysis. A comprehensive description of the PHENIX detector is documented elsewhere [27]. The analysis described here utilizes the central spectrometer arms, which consist of a set of tracking detectors [28], particle identification detectors [29], and an electromagnetic calorimeter [30]. The central spectrometer arms cover a rapidity range of $|\eta| < 0.35$, and each arm subtends 90° in azimuth. A detailed description of the algorithms and performance of the central arm track reconstruction and momentum reconstruction can be found in Ref. [31].

There are two detectors that are used for triggering, centrality determination, and event vertex determination. The beam-beam counters (BBCs) consist of 64 individual quartz Cherenkov counters that cover the full azimuthal angle in the pseudorapidity range $3.0 < |\eta| < 3.9$. The zero degree calorimeters (ZDCs) cover the pseudorapidity range $|\eta| > 6$ and measure the energy of spectator neutrons with an energy resolution of approximately 20%. More details about these detectors can be found in Ref. [32]. The collision vertex position is determined using timing information from the BBCs with an r.m.s. resolution for central Au+Au events of 6 mm along the beam axis. The collision vertex is required to be reconstructed within ± 30 cm from the center of the spectrometer. The BBCs also provide a minimum-bias (MB) event trigger.

Because of the large dynamic range in $\sqrt{s_{NN}}$ covered by this analysis, it is necessary to implement algorithms that are dependent on the collision energy for the determination of the centrality of each event. In Au+Au collisions at $\sqrt{s_{NN}} =$ 200 GeV, the centrality of the collision is determined by using correlations of the total energy deposited in the ZDCs with the total charge deposited in the BBCs as described in Ref. [33]. However, in 200 GeV Cu+Cu, 62.4 GeV Cu+Cu, and 62.4 GeV Au+Au collisions, the resolving power of the ZDCs is insufficient to significantly contribute to the centrality definition. Therefore, only the total charge deposited in the BBCs is used to determine centrality in these collision systems, as described in Ref. [33]. Using the 200 GeV Au+Au data, it has been verified that application of the BBC-ZDC correlation for the centrality definition as opposed to the BBC-only definition shows no significant differences in the values of the charged hadron fluctuation quantities presented here as a function of centrality.

The location of the BBCs are fixed for every collision energy. At the lowest collision energy ($\sqrt{s_{NN}} = 22.5$ GeV), it becomes kinematically possible for spectator nucleons to fall within the acceptance of the BBC. This results in a BBC response in its total charge sum that is no longer linear with the number of participating nucleons ($N_{\rm part}$). In this case, it becomes necessary to define the centrality using the total charged particle multiplicity in pad chamber 1 (PC1) [28]. PC1 is chosen because of its fine segmentation, high tracking efficiency, and relative proximity to the event vertex. Details on this procedure are also described in Ref. [33]. For all collision species and energies, the distribution of the number of participants was determined using a Monte Carlo simulation based upon the Glauber model [33,34].

The number of minimum-bias events analyzed for each dataset are 25.6×10^6 events for 200 GeV Au+Au, 24.9×10^6 events for 62.4 GeV Au+Au, 15.0×10^6 events for 200 GeV Cu+Cu, 12.2×10^6 events for 62.4 GeV Cu+Cu, 5.5×10^6 events for 22.5 GeV Cu+Cu, and 2.7×10^6 events for 200 GeV $p+p$. Only a fraction of the complete 200 GeV Au+Au, Cu+Cu, and $p+p$ datasets are analyzed, but this fraction is more than sufficient for this analysis.

The charged particle multiplicity is determined on an event-by-event basis by counting the number of unambiguous reconstructed tracks in the drift chamber originating from the collision vertex that have corresponding hits in PC1 and PC3. Track selection includes cuts on reconstructed tracks in the drift chamber to reduce double-counted ghost tracks to a negligible level. To minimize background originating from the magnets, reconstructed tracks are required to lie within ± 75 cm from the center of the drift chamber along the beam axis. This requirement reduces the pseudorapidity range of reconstructed tracks to $|\eta| < 0.26$. The ring imaging Cherenkov detector (RICH) is utilized to reduce background from electrons resulting from photon conversions.

Although the central arm spectrometer covers a total azimuthal range of π radians, detector and tracking inefficiencies reduce the effective average azimuthal active area to 2.1 radians for the 200 Gev Au+Au and 200 GeV $p+p$ datasets, and 2.0 radians for the other datasets. Fluctuation quantities are quoted for these acceptances separately for each dataset. The differences in acceptance between datasets, which are due to variations in the detector over the three-year period in which the data were collected, result in less than a 1% variation in the fluctuation quantities quoted here.

III. DATA ANALYSIS

Multiplicity fluctuations of charged particles, designated $\omega_{\rm ch}$, can be generally defined [35] as

$$\omega_{\rm ch} = \frac{\langle N_{\rm ch}^2 \rangle - \langle N_{\rm ch} \rangle^2}{\langle N_{\rm ch} \rangle} = \frac{\sigma_{\rm ch}^2}{\mu_{\rm ch}}, \tag{5}$$

where $N_{\rm ch}$ is the charged particle multiplicity. Simply stated, the fluctuations can be quoted as the variance of the multiplicity ($\sigma_{\rm ch}^2$) normalized by the mean ($\mu_{\rm ch} = \langle N_{\rm ch} \rangle$). This is also referred to as the scaled variance [25]. If the multiplicity distribution is Poissonian, the scaled variance is 1.0.

It has been well established that charged particle multiplicity distributions in elementary nucleon-nucleon collisions can be described by the negative binomial distribution (NBD) [17–19]. The NBD also describes well the multiplicity distributions in heavy ion collisions [21,23]. The NBD of an integer n is defined as

$$P(n) = \frac{\Gamma(n + k_{\rm NBD})}{\Gamma(n+1)\Gamma(k_{\rm NBD})} \frac{(\mu_{\rm ch}/k_{\rm NBD})^n}{(1 + \mu_{\rm ch}/k_{\rm NBD})^{n+k_{\rm NBD}}}, \tag{6}$$

where $P(n)$ is normalized to 1.0 over the range $0 \leqslant n \leqslant \infty$, $\mu_{\rm ch} = \langle N_{\rm ch} \rangle = \langle n \rangle$, and $k_{\rm NBD}$ is an additional parameter. The NBD reduces to a Poisson distribution in the limit $k_{\rm NBD} \to \infty$. The NBD variance and mean is related to $k_{\rm NBD}$ as follows:

$$\frac{\sigma_{\rm ch}^2}{\mu_{\rm ch}^2} = \frac{\omega_{\rm ch}}{\mu_{\rm ch}} = \frac{1}{\mu_{\rm ch}} + \frac{1}{k_{\rm NBD}}. \tag{7}$$

Hence, the scaled variance is given by

$$\omega_{\rm ch} = 1 + \frac{\mu_{\rm ch}}{k_{\rm NBD}}. \tag{8}$$

A useful property of the negative binomial distribution concerns its behavior when a population that follows the NBD is subdivided randomly by repeated independent trials with a constant probability onto smaller subsets. This results in a binomial decomposition of the original population into subsets that also follow the NBD with the same value of $k_{\rm NBD}$ [21]. This property can be applied to estimate the behavior of multiplicity fluctuations as a function of acceptance, assuming that there are no significant correlations present over the acceptance range being examined. Starting with an original NBD sample with mean $\mu_{\rm ch}$ and scaled variance $\omega_{\rm ch}$, a sample in a fractional acceptance with mean $\mu_{\rm acc}$ is also described by an NBD distribution. An acceptance fraction can be defined as $f_{\rm acc} = \mu_{\rm acc}/\mu_{\rm ch}$. The scaled variance of the subsample from Eq. (8) is thus

$$\omega_{\rm acc} = 1 + (\mu_{\rm acc}/k_{\rm NBD}) = 1 + (f_{\rm acc}\mu_{\rm ch}/k_{\rm NBD}). \tag{9}$$

Since $k_{\rm NBD}$ is identical for the two samples, $\mu_{\rm ch}/k_{\rm NBD} = \omega_{\rm ch} - 1$ can be substituted, yielding the following relation between

TABLE I. Tabulation of the charged hadron multiplicity data and corrections for $0.2 < p_T < 2.0$ GeV/c. The errors quoted for $\mu_{\rm ch}$ and $\sigma_{\rm ch}$ represent their time-dependent systematic error. The errors quoted for $\omega_{\rm ch,dyn}$ and $1/k_{\rm NBD,dyn}$ represent their total systematic error. For each dataset, the first three columns give the species, collision energy, and geometric correction factor $f_{\rm geo}$, respectively.

Species	$\sqrt{s_{NN}}$ (GeV)	$f_{\rm geo}$	$N_{\rm part}$	$\mu_{\rm ch}$	Raw $\sigma^2_{\rm ch}$	$\omega_{\rm ch,dyn}$	$1/k_{\rm NBD,dyn}$	χ^2/dof
			351	61.0 ± 1.1	75.6 ± 1.9	1.10 ± 0.02	$1.45 \times 10^{-03} \pm 2.2 \times 10^{-04}$	37.1/58
			299	53.1 ± 1.0	71.8 ± 1.8	1.15 ± 0.02	$2.45 \times 10^{-03} \pm 2.7 \times 10^{-04}$	38.6/56
			253	45.8 ± 0.8	65.2 ± 1.5	1.17 ± 0.02	$3.41 \times 10^{-03} \pm 2.9 \times 10^{-04}$	34.0/54
			215	39.1 ± 0.7	57.8 ± 1.6	1.19 ± 0.03	$4.53 \times 10^{-03} \pm 3.6 \times 10^{-04}$	29.1/53
			181	32.6 ± 0.6	49.7 ± 1.3	1.21 ± 0.03	$5.95 \times 10^{-03} \pm 5.1 \times 10^{-04}$	24.5/50
Au+Au	200	0.37 ± 0.027	151	27.4 ± 0.5	41.4 ± 1.0	1.20 ± 0.03	$6.86 \times 10^{-03} \pm 5.5 \times 10^{-04}$	20.7/46
			125	22.3 ± 0.4	33.8 ± 0.9	1.20 ± 0.03	$8.47 \times 10^{-03} \pm 7.1 \times 10^{-04}$	11.9/41
			102	17.8 ± 0.3	26.7 ± 0.6	1.19 ± 0.02	$1.05 \times 10^{-02} \pm 9.0 \times 10^{-04}$	16.6/37
			82	14.2 ± 0.3	20.8 ± 0.6	1.17 ± 0.02	$1.20 \times 10^{-02} \pm 1.0 \times 10^{-03}$	37.8/33
			65	10.8 ± 0.2	16.0 ± 0.4	1.18 ± 0.02	$1.64 \times 10^{-02} \pm 1.3 \times 10^{-03}$	37.8/28
			51	8.3 ± 0.2	12.1 ± 0.3	1.17 ± 0.02	$2.06 \times 10^{-02} \pm 2.0 \times 10^{-03}$	53.8/24
			345	44.0 ± 0.3	53.6 ± 0.5	1.08 ± 0.02	$1.63 \times 10^{-03} \pm 2.0 \times 10^{-04}$	14.6/54
			296	37.3 ± 0.2	48.3 ± 0.3	1.11 ± 0.02	$2.63 \times 10^{-03} \pm 2.6 \times 10^{-04}$	13.8/53
			250	31.0 ± 0.2	39.8 ± 0.4	1.10 ± 0.02	$3.00 \times 10^{-03} \pm 3.0 \times 10^{-04}$	14.0/50
			211	25.4 ± 0.2	33.6 ± 0.5	1.12 ± 0.02	$4.21 \times 10^{-03} \pm 4.4 \times 10^{-04}$	8.36/44
			177	20.8 ± 0.1	27.8 ± 0.2	1.12 ± 0.02	$5.34 \times 10^{-03} \pm 5.5 \times 10^{-04}$	19.2/40
Au+Au	62.4	0.33 ± 0.031	148	16.6 ± 0.1	22.8 ± 0.3	1.13 ± 0.02	$7.43 \times 10^{-03} \pm 7.8 \times 10^{-04}$	25.9/37
			123	13.1 ± 0.1	18.1 ± 0.2	1.13 ± 0.02	$9.61 \times 10^{-03} \pm 9.7 \times 10^{-04}$	34.3/33
			102	10.4 ± 0.1	14.9 ± 0.1	1.15 ± 0.02	$1.38 \times 10^{-02} \pm 1.4 \times 10^{-03}$	44.5/28
			82	7.8 ± 0.1	11.1 ± 0.1	1.14 ± 0.02	$1.76 \times 10^{-02} \pm 1.9 \times 10^{-03}$	50.9/24
			66	5.9 ± 0.04	8.3 ± 0.1	1.14 ± 0.02	$2.37 \times 10^{-02} \pm 3.8 \times 10^{-03}$	45.4/20
			51	4.1 ± 0.03	5.8 ± 0.04	1.13 ± 0.02	$3.08 \times 10^{-02} \pm 9.1 \times 10^{-03}$	36.2/17
			104	19.3 ± 0.3	25.7 ± 0.8	1.14 ± 0.03	$6.93 \times 10^{-03} \pm 1.3 \times 10^{-03}$	24.3/30
			92	16.0 ± 0.2	21.9 ± 0.5	1.15 ± 0.03	$9.26 \times 10^{-03} \pm 1.5 \times 10^{-03}$	21.7/31
			79	13.5 ± 0.2	18.8 ± 0.4	1.16 ± 0.03	$1.15 \times 10^{-02} \pm 2.1 \times 10^{-03}$	19.4/29
Cu+Cu	200	0.40 ± 0.047	67	11.1 ± 0.2	15.3 ± 0.3	1.15 ± 0.03	$1.36 \times 10^{-02} \pm 2.0 \times 10^{-03}$	29.9/26
			57	9.2 ± 0.1	13.0 ± 0.3	1.17 ± 0.03	$1.75 \times 10^{-02} \pm 2.5 \times 10^{-03}$	26.0/25
			48	7.5 ± 0.1	10.5 ± 0.2	1.16 ± 0.03	$2.14 \times 10^{-02} \pm 3.6 \times 10^{-03}$	30.6/22
			40	6.2 ± 0.1	8.7 ± 0.2	1.17 ± 0.03	$2.69 \times 10^{-02} \pm 4.8 \times 10^{-03}$	28.6/20
			33	4.9 ± 0.06	6.8 ± 0.1	1.16 ± 0.03	$3.12 \times 10^{-02} \pm 8.5 \times 10^{-03}$	45.7/18
			104	12.6 ± 0.1	16.7 ± 0.2	1.10 ± 0.03	$8.16 \times 10^{-03} \pm 1.7 \times 10^{-03}$	40.6/31
			92	11.0 ± 0.1	16.2 ± 0.1	1.15 ± 0.04	$1.35 \times 10^{-02} \pm 2.7 \times 10^{-03}$	64.2/30
Cu+Cu	62.4	0.32 ± 0.063	79	9.2 ± 0.1	14.3 ± 0.2	1.18 ± 0.05	$1.92 \times 10^{-02} \pm 3.9 \times 10^{-03}$	37.0/28
			67	7.7 ± 0.1	12.0 ± 0.2	1.18 ± 0.05	$2.29 \times 10^{-02} \pm 4.6 \times 10^{-03}$	32.0/26
			57	6.0 ± 0.1	9.1 ± 0.1	1.17 ± 0.05	$2.85 \times 10^{-02} \pm 5.9 \times 10^{-03}$	32.0/23
			48	5.1 ± 0.1	8.1 ± 0.1	1.19 ± 0.05	$3.66 \times 10^{-02} \pm 8.0 \times 10^{-03}$	29.2/21
			92	9.1 ± 0.04	10.3 ± 0.1	1.04 ± 0.02	$4.31 \times 10^{-03} \pm 9.8 \times 10^{-04}$	7.45/24
Cu+Cu	22.5	0.30 ± 0.064	58	4.9 ± 0.02	5.8 ± 0.04	1.06 ± 0.02	$1.11 \times 10^{-02} \pm 2.9 \times 10^{-03}$	71.1/17

the scaled variances of the original and fractional acceptance samples:

$$\omega_{\rm acc} = 1 + f_{\rm acc}(\omega_{\rm ch} - 1). \quad (10)$$

Thus, the measured scaled variance will decrease as the acceptance is decreased, while $k_{\rm NBD}$ remains constant, if there are no additional correlations present over the given acceptance range.

Figures 1 and 2 show the uncorrected, or raw, multiplicity distributions in the p_T range $0.2 < p_T < 2.0$ GeV for all centralities from each collision system overlaid with fits to negative binomial distributions (dashed lines). For presentation purposes, the data have been normalized on the horizontal axis by the mean of the distribution and scaled on the vertical axis by the successive amounts stated in the legend. The NBD fits describe the data distributions very well for all collision systems, centralities, and p_T ranges. Hence, the mean and variance of the multiplicity distributions presented here are all extracted from NBD fits. The results of each fit for $0.2 < p_T < 2.0$ GeV are compiled in Table I. The mean and standard deviation of each fit for $0.2 < p_T < 2.0$ GeV are plotted in Fig. 3.

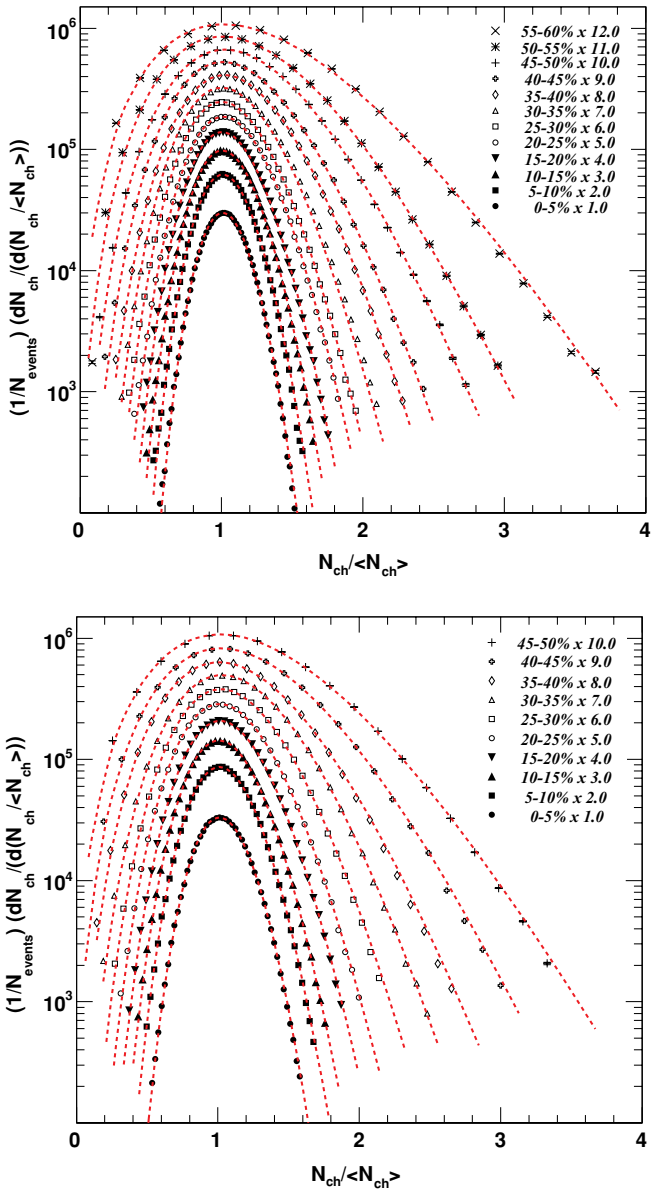

FIG. 1. (Color online) Uncorrected multiplicity distributions of charged hadrons with $0.2 < p_T < 2.0$ GeV/c for 200 (upper) and 62.4 (lower) GeV Au+Au collisions. The dashed lines are fits to the NBD. The data are normalized to the mean and scaled by the amounts in the legend.

Each dataset was taken over spans of several days to several weeks, all spanning three separate RHIC running periods. During these periods, changes in the total acceptance and efficiency of the central arm spectrometers cause the fluctuation measurements to vary, thus introducing an additional systematic error to the results. This systematic error was minimized by requiring that the dataset is stable in quantities that are sensitive to detector variations, including the mean charged particle multiplicity, mean collision vertex position, and mean centrality. A time-dependent systematic error is applied independently to each point by calculating the standard deviation of the scaled variance calculated from subsets of the entire dataset, with each subset containing about 1×10^6

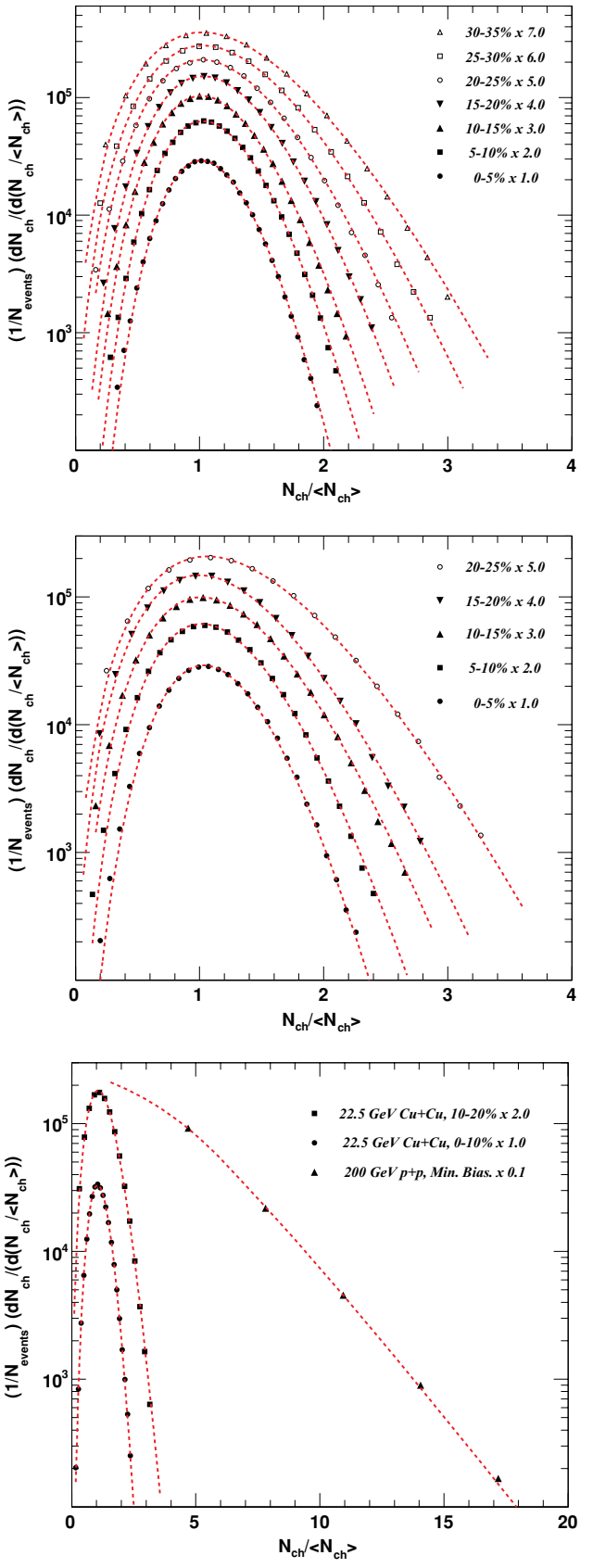

FIG. 2. (Color online) Same as Fig. 1, but for 200 (upper), 62.4 (middle), and 22.5 (lower) GeV Cu+Cu and 200 GeV $p+p$ (lower) collisions.

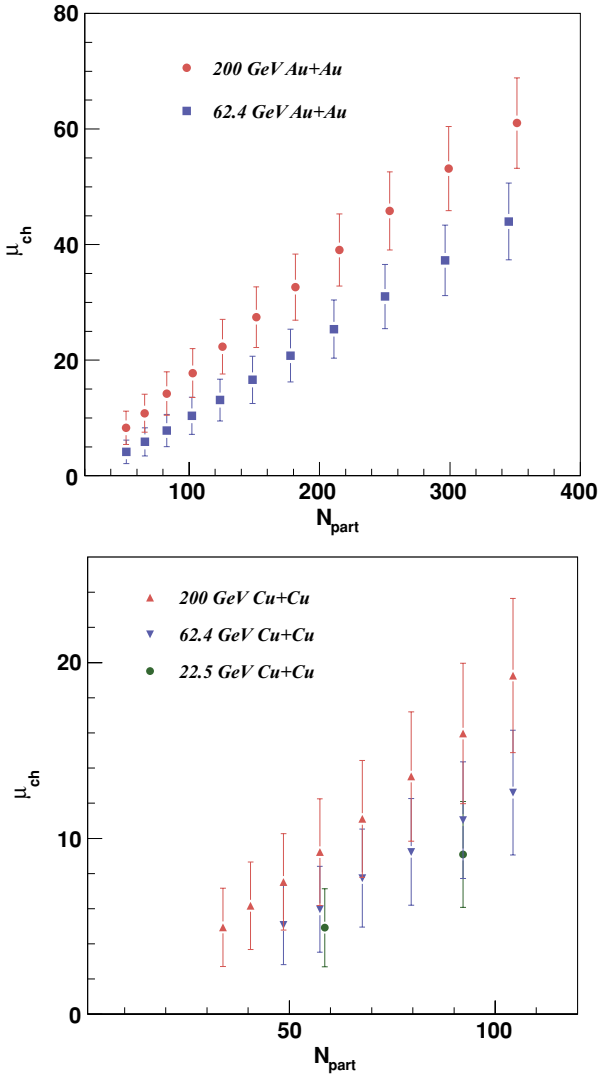

FIG. 3. (Color online) Mean from the NBD fit as a function of N_{part} for Au+Au (upper) and Cu+Cu (lower) collisions over the range $0.2 < p_T < 2.0\,\text{GeV}/c$. The mean shown is within the PHENIX central arm spectrometer acceptance. The error bars represent the standard deviation of the distribution.

events. These systematic errors are applied to all subsequent results.

The tracking efficiency of the PHENIX central arm spectrometer is dependent on centrality, especially in the most central 200 GeV Au+Au collisions [36]. With the assumption that tracking inefficiencies randomly affect the multiplicity distribution on an event-by-event basis, the effect of inefficiencies on the scaled variance can be estimated using Eq. (10), where f_{acc} is replaced by the inverse of the tracking efficiency $1/f_{\text{eff}}$. Tracking efficiency affects the value of the scaled variance by 1.5% at the most. The scaled variance has been corrected for tracking inefficiency as a function of centrality for all species. The uncertainty of the tracking efficiency estimate is typically 2% and has been propagated into the systematic error estimate on a point-by-point basis.

Because of the nonzero width of the centrality bin selection from the data, each centrality bin necessarily selects a range of impact parameters. This introduces a nondynamical fluctuation component to the measured multiplicity fluctuations due to the resulting fluctuations in the geometry of the collisions [26,37]. Therefore, it is necessary to estimate the magnitude of the geometry fluctuation component so that only the interesting dynamical fluctuations remain. The most practical method for estimating the geometry fluctuation component is with a model of heavy ion collisions. The URQMD [38] and HSD [39,40] models have previously been applied for this purpose. Here, the HIJING event generator [41] is chosen for this estimate, because it reproduces well the mean multiplicity in heavy ion collisions [33] as measured by the PHENIX detector. HIJING includes multiple minijet production based upon QCD-inspired models, soft excitation, nuclear shadowing of parton distribution functions, and the interaction of jets in dense nuclear matter. The estimate is performed individually for each centrality bin, collision system, and p_T range using the following procedure. First, HIJING is run with an impact parameter distribution that is sampled from a Gaussian distribution with a mean and standard deviation that, for a given centrality bin, reproduces the distributions of the charge deposited in the BBC and the energy deposited in the ZDC (for 200 GeV Au+Au). Second, HIJING is run at a fixed impact parameter with a value identical to the mean of the Gaussian distribution in the first run. For each centrality bin, 12,000 HIJING events are processed for each impact parameter selection. The scaled variance for each impact parameter selection, ω_{Gauss} and ω_{fixed}, is extracted and the measured scaled variance is corrected as the fractional deviation from a scaled variance of 1.0 of a Poisson distribution as follows:

$$\omega_{\text{ch,dyn}} - 1 = \frac{\omega_{\text{fixed}} - 1}{\omega_{\text{Gauss}} - 1}(\omega_{\text{ch,raw}} - 1) = f_{\text{geo}}(\omega_{\text{ch,raw}} - 1), \tag{11}$$

where $\omega_{\text{ch,dyn}}$ represents the estimate of the remaining dynamical multiplicity fluctuations and $\omega_{\text{ch,raw}}$ represents the uncorrected multiplicity fluctuations. Since the correction f_{geo} is calculated as a ratio of the two running conditions of the simulation, most multiplicity fluctuations intrinsic to the model should be canceled. The correction always reduces the magnitude of the measured scaled variance. Note that the value of f_{geo} is mathematically identical when applied to the inverse of k_{NBD}:

$$k^{-1}_{\text{NBD,dyn}} = f_{\text{geo}} k^{-1}_{\text{NBD}}. \tag{12}$$

The resulting geometrical correction factors for each species are constant as a function of centrality, therefore a single correction factor is calculated for each transverse momentum range by fitting the correction factors as a function of N_{part} to a constant. This behavior is expected, since centrality bins are defined to be constant percentages of the total geometric cross section. The correction factors for each transverse momentum range for a given collision species are consistent with each other, that is, they are independent of transverse momentum. The standard deviation of the individual geometrical correction factors from the linear fits as a function of N_{part} are included in the systematic error of the correction factor estimation and propagated

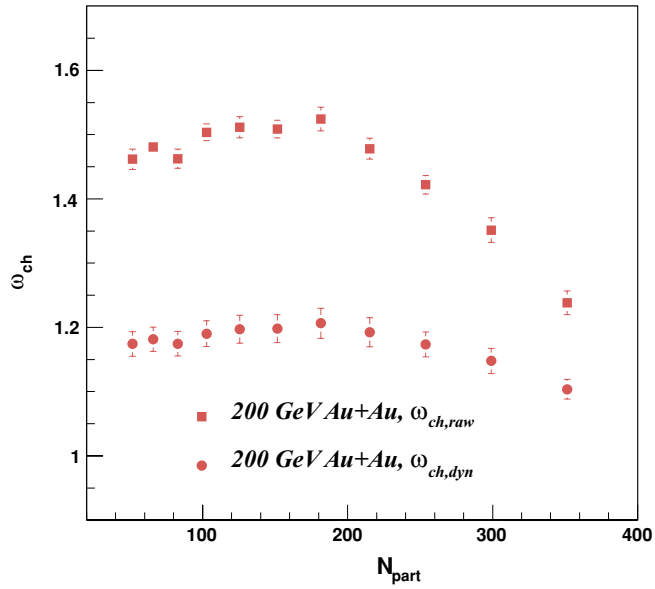

FIG. 4. (Color online) Fluctuations expressed as the scaled variance as a function of centrality for 200 GeV Au+Au collisions in the range $0.2 < p_T < 2.0$ GeV/c. Shown are the uncorrected fluctuations, $\omega_{\mathrm{ch,raw}}$, along with fluctuations after correcting for the estimated contribution from geometry fluctuations using Eq. (11), $\omega_{\mathrm{ch,dyn}}$.

into the total systematic error for each point in $\omega_{\mathrm{ch,dyn}}$ and $k_{\mathrm{NBD,dyn}}$. For $0.2 < p_T < 2.0$ GeV/c, the geometrical correction factors f_{geo} and systematic errors from the fit are 0.37 ± 0.027 for 200 GeV Au+Au, 0.33 ± 0.031 for 62.4 GeV Au+Au, 0.40 ± 0.047 for 200 GeV Cu+Cu, 0.32 ± 0.063 for 62.4 GeV Cu+Cu, and 0.30 ± 0.064 for 22.5 GeV Cu+Cu. The extraction of the geometrical correction factors are inherently model dependent and are also dependent on the accuracy with which the centrality detectors are modeled. The effect of the latter dependence has been studied by also calculating the correction factors using constant but nonoverlapping impact parameter distributions for each centrality bin and comparing them with the correction factors using the Gaussian impact parameter distributions. For all p_T ranges, an additional fraction of the value of $\omega_{\mathrm{ch,dyn}}$ or $k^{-1}_{\mathrm{NBD,dyn}}$ has been included in the final systematic errors for these quantities. The magnitude of this systematic error is 8% for 200 GeV Au+Au, 8% for 62.4 GeV Au+Au, 11% for 200 GeV Cu+Cu, 17% for 62.4 GeV Cu+Cu, and 25% for 22.5 GeV Cu+Cu. A sample comparison of the scaled variance before and after the application of the geometrical correction factor is shown for the 200 GeV Au+Au dataset in Fig. 4.

IV. RESULTS

The scaled variance as a function of the number of participating nucleons N_{part} over the p_T range $0.2 < p_T < 2.0$ GeV/c is shown in Fig. 5. For all centralities, the scaled variance values consistently lie above the Poisson distribution value of 1.0. In all collision systems, the minimum scaled variance occurs in the most central collisions and then begins to increase as the centrality decreases. In 200 GeV Au+Au

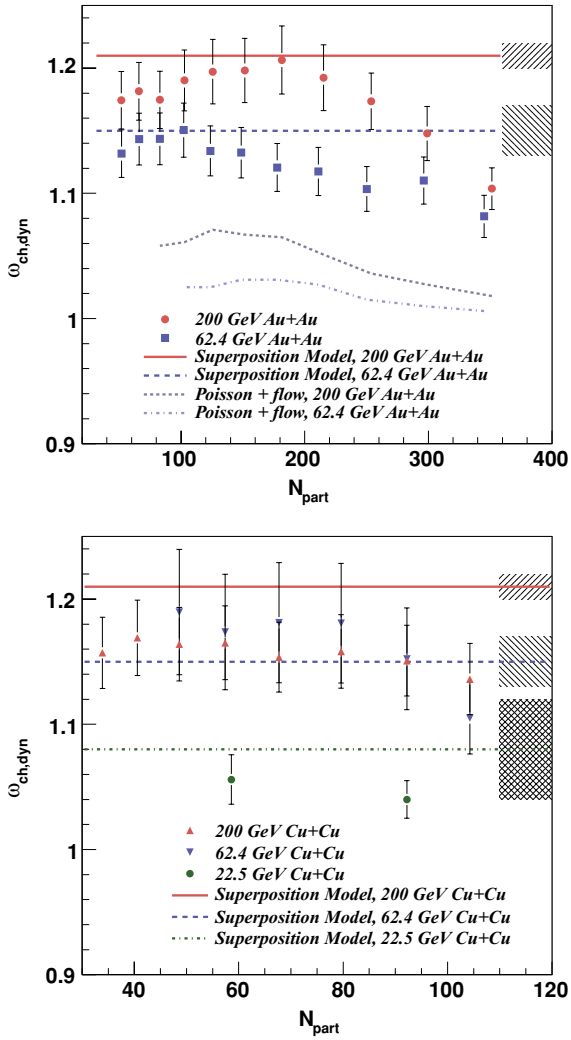

FIG. 5. (Color online) Fluctuations expressed as the scaled variance as a function of N_{part} for Au+Au (upper) and Cu+Cu (lower) collisions for $0.2 < p_T < 2.0$ GeV/c. The estimated contribution from geometry fluctuations has been removed. Results from the superposition model are overlaid with the shaded regions representing a one standard deviation range of the prediction for the fluctuation magnitude derived from $p+p$ collision data. Also shown (upper) is the estimated contribution from noncorrelated particle emission with the Poisson distribution of the scaled variance of 1.0 with the addition of elliptic flow in 200 and 62 GeV Au+Au collisions.

collisions, this increase is only observed for $N_{\mathrm{part}} > 200$. For $N_{\mathrm{part}} < 200$, the magnitude of $\omega_{\mathrm{ch,dyn}}$ suggests a slight decrease but is consistent with a constant value. In 62.4 GeV Au+Au collisions, the increase in $\omega_{\mathrm{ch,dyn}}$ with decreasing centrality is observed only over the range $N_{\mathrm{part}} > 110$. The source of the qualitative differences between the 200 and 62.4 GeV Au+Au collisions are not known, although some of the differences could be explained by the increased contribution from hard scattering processes at 200 GeV compared to 62.4 GeV. Studies performed by varying the centrality selection cuts establish that the differences are not due to the differences in the centrality selection algorithm. A similar centrality-dependent trend of the scaled variance has also been observed at the

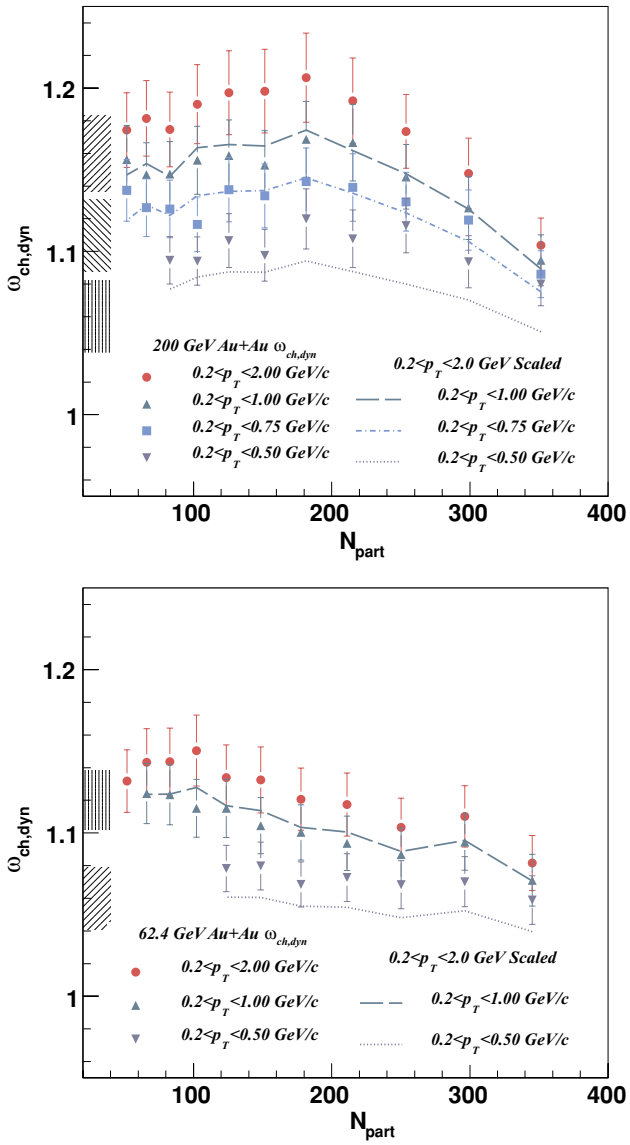

FIG. 6. (Color online) Scaled variance for 200 and 62.4 GeV Au+Au collisions plotted as a function of N_{part} for several p_T ranges. The lines represent the data for the reference range $0.2 < p_T < 2.0$ scaled down using the mean multiplicity in each successive p_T range. The shaded areas represent the systematic errors from the reference range.

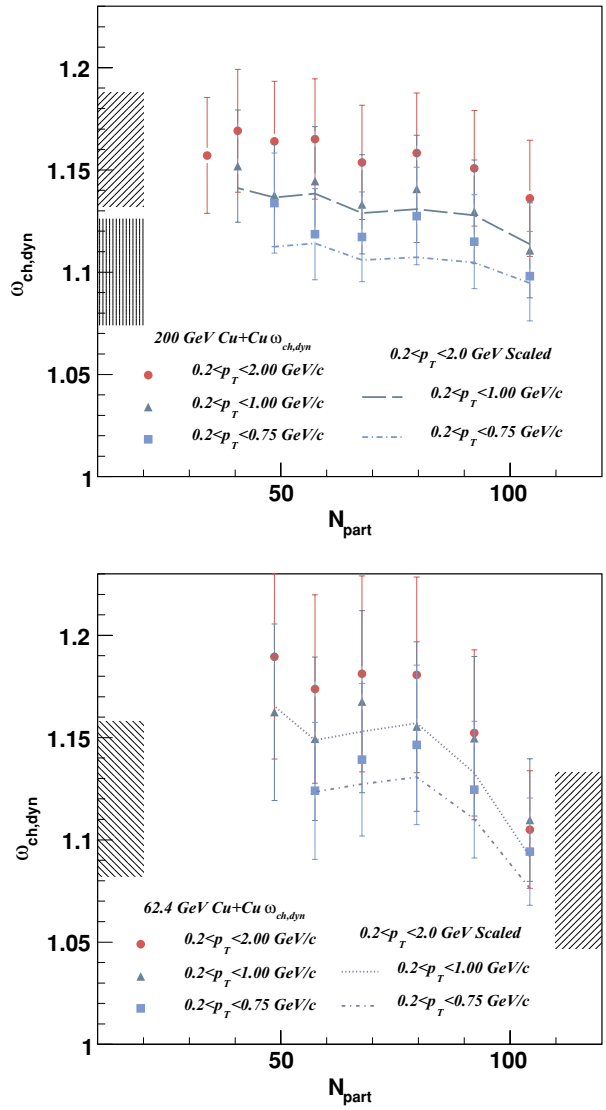

FIG. 7. (Color online) Same as Fig. 6, but for Cu+Cu collisions.

CERN Super Proton Synchrotron (SPS) in low-energy Pb+Pb collisions at $\sqrt{s_{NN}} = 17.3$ GeV and at forward rapidities ($1.1 < y_{\text{c.m.}} < 2.6$), measured by experiment NA49 [25], where the hard scattering contribution is expected to be small. The 200 GeV Cu+Cu data exhibit a weaker decrease in the scaled variance for more central collisions. The 62.4 GeV Cu+Cu scaled variance values are consistently above those from the 200 GeV Cu+Cu dataset, but the two are consistent within the systematic errors for all centralities.

The scaled variance has been studied as a function of the p_T range over which the multiplicity distributions are measured in order to determine if any significant p_T-dependent dynamical fluctuations are present. Results for several p_T ranges from $0.2 < p_T < 2.0$ down to $0.2 < p_T < 0.5$ GeV/c are shown in Figs. 6 and 7. In the absence of p_T-dependent dynamical fluctuations, restricting the p_T range should reduce the scaled variance in the same manner as for a fractional acceptance. Similar to Eq. (10),

$$\omega_{p_T} = 1 + f_{p_T}(\omega_{\text{ref}} - 1), \tag{13}$$

where ω_{p_T} represents the fluctuations in the p_T range of interest, ω_{ref} represents the fluctuations in the reference p_T range, and $f_{p_T} = \mu_{p_T}/\mu_{\text{ref}}$ is the ratio of the mean multiplicity in the two ranges. Also shown are curves representing the expected scaling of the fluctuations using the range $0.2 < p_T < 2.0$ GeV/c as the reference range. The shaded regions reflect the systematic errors of the reference range. For all p_T ranges, the scaled fluctuation curves are consistent with the data, indicating that no significant p_T dependence is observed, although the data in the range $0.2 < p_T < 0.5$ GeV are consistently above the scaled reference curves. The p_T dependence can also be examined more directly with the parameter k_{NBD} from the NBD fits. Substitution of the scaled variance in Eq. (8) into Eq. (13) shows that k_{NBD} should be

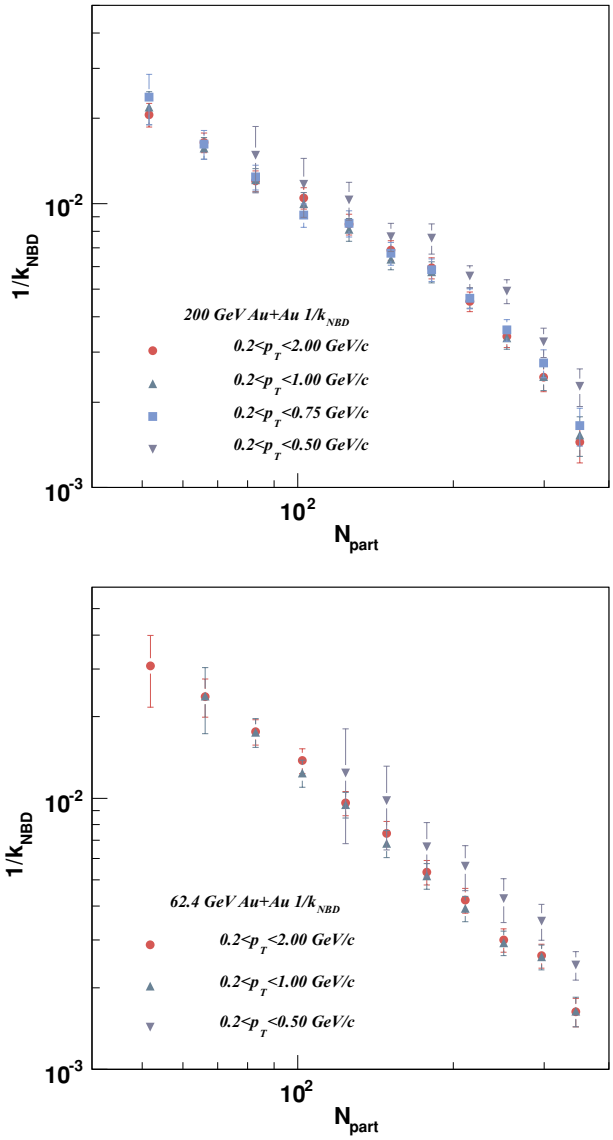

FIG. 8. (Color online) Inverse of the parameter k_{NBD} from the NBD fits for 200 and 62.4 GeV Au+Au collisions. The fluctuations are plotted as a function of N_{part} for several p_T ranges.

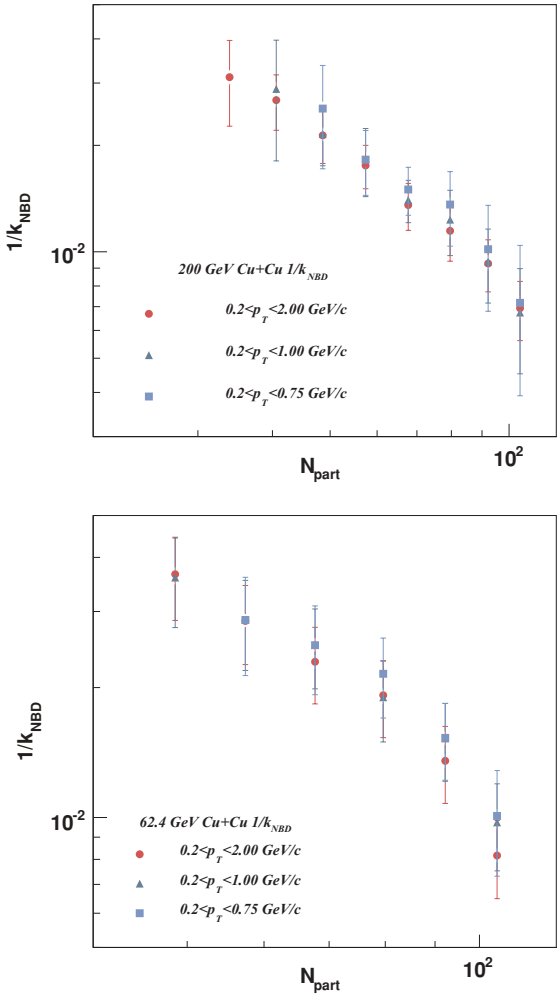

FIG. 9. (Color online) Same as Fig. 8, but for Cu+Cu collisions.

independent of p_T in the absence of p_T-dependent dynamical fluctuations. As shown in Figs. 8 and 9, there is no significant p_T-dependence of the observed values of k_{NBD}.

The scaled variance as a function of the charge sign of the charged hadrons is shown in Fig. 10 for 200 GeV Au+Au collisions in the p_T range $0.2 < p_T < 2.0$ GeV/c in order to investigate any Coulomb-based contributions to the fluctuations. In the absence of additional dynamic fluctuations, the scaled variance for positively or negatively charged hadrons should be reduced from the inclusive charged hadron value by

$$\omega_{+-} = 1 + f_{+-}(\omega_{\mathrm{ch}} - 1), \tag{14}$$

where ω_{+-} are the fluctuations for positive or negative particles, ω_{ch} are the fluctuations for inclusive charged hadrons, and $f_{+-} = \mu_{+-}/\mu_{\mathrm{ch}}$ is the ratio of the mean multiplicities. The scaled variance from the positive and negative hadrons are consistent with each other and with the expected reduction of the inclusive charged hadron fluctuations.

V. DISCUSSION

A. Comparisons with a participant superposition model

It is informative to compare fluctuations in relativistic heavy ion collisions to what can be expected from the superposition of individual participant nucleon-nucleon collisions. For this purpose, PHENIX data will be compared with a participant superposition, or wounded nucleon, model [42] based upon data from elementary collisions. In the participant superposition model, the total multiplicity fluctuations can be expressed in terms of the scaled variance [35],

$$\omega_{\mathrm{N}} = \omega_{\nu} + \mu_{\mathrm{WN}}\omega_{N_{\mathrm{part}}}, \tag{15}$$

where ω_{ν} are the fluctuations from each individual source, e.g., from each elementary collision, $\omega_{N_{\mathrm{part}}}$ are the fluctuations of the number of sources, and μ_{WN} is the mean multiplicity per wounded nucleon. The second term includes nondynamic contributions from geometry fluctuations due to the width of the centrality bin along with additional fluctuations in the number of participants for a fixed impact parameter. Ideally, the second term is nearly nullified after applying the geometry

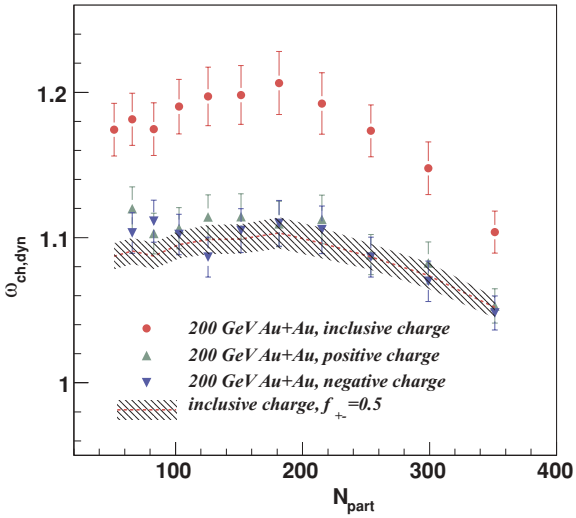

FIG. 10. (Color online) Scaled variance as a function of N_{part} for 200 GeV Au+Au collisions in the range $0.2 < p_T < 2.0$ GeV/c. Shown are measurements for inclusive charged particles, positive particles, and negative particles. The line represents the inclusive data scaled down in acceptance by 50% with the shaded area representing the systematic error.

corrections described previously, so the resulting fluctuations are independent of centrality as well as collision species.

Baseline comparisons are facilitated by PHENIX measurements of charged particle multiplicity fluctuations in minimum-bias 200 GeV $p+p$ collisions. The $p+p$ data and the NBD distribution to the multiplicity distribution are shown in Fig. 2. The NBD fit yields $\mu_{\text{ch}} = 0.32 \pm 0.003$, $\omega_{\text{ch}} = 1.17 \pm 0.01$, and $k_{\text{NBD}} = 1.88 \pm 0.01$. These results are in agreement within errors with previous measurements in the same pseudorapidity range of $k_{\text{NBD}} = 1.9 \pm 0.2 \pm 0.2$ by the UA5 Collaboration [20] in collisions of protons and antiprotons at 200 GeV. Comparisons between the participant superposition model predictions and the 22.5 GeV Cu+Cu data can be made using multiplicity fluctuations measured in 20 GeV $p+p$ collisions by the NA22 Collaboration [19] over the same pseudorapidity range as the PHENIX Cu+Cu measurement. After scaling the NA22 scaled variance to the PHENIX azimuthal acceptance, the participant superposition model scaled variance is expected to be constant as a function of centrality with a value of 1.08 ± 0.04. Lacking multiplicity distribution data from elementary collisions at 62.4 GeV within the PHENIX pseudorapidity acceptance, it is assumed that as a function of collision energy, the scaled variance in the PHENIX pseudorapidity acceptance scales in the same manner as in an acceptance of 4π, which can be parametrized from existing $p+p$ and $p+\bar{p}$ data as follows [17]:

$$\mu_{\text{ch}} \approx -4.2 + 4.69 \left(\frac{s}{\text{GeV}^2} \right)^{0.155}. \tag{16}$$

Given the mean charged particle multiplicity, the scaled variance in $p+p$ and $p+\bar{p}$ can be parametrized as follows [35]:

$$\omega_{\text{ch}} \approx 0.35 \frac{(\mu_{\text{ch}} - 1)^2}{\mu_{\text{ch}}}. \tag{17}$$

Scaling this parametrization to match the values of ω_{ch} at 200 and 22.5 GeV, the estimated value of ω_{ch} at 62.4 GeV is 1.15 ± 0.02.

Comparisons of the data with the predictions of the participant superposition model are shown in Fig. 5 for Au+Au and Cu+Cu collisions. The shaded regions about the participant superposition model lines represent the systematic error of the estimates described above. All of the data points are consistent with or below the participant superposition model estimate. This suggests that the data do not show any indications of the presence of a critical point, where the fluctuations are expected to be much larger than the participant superposition model expectation.

B. Comparisons to the HIJING model

Shown in Fig. 11 are the scaled variance curves from HIJING simulations into the PHENIX acceptance. The HIJING simulations are performed with a fixed impact parameter corresponding to the mean of the impact parameter distribution for each bin as determined by the Glauber model in order to minimize the geometry fluctuation component of the result. The mean and variance of the resulting multiplicity distributions from HIJING are extracted from fits to negative binomial distributions. The HIJING simulation multiplicity fluctuations with the jet production parameter turned on are consistently above the data and increase continuously through the most peripheral collisions. This behavior is not consistent with the data, where the fluctuations do not increase in the most peripheral collisions. Although HIJING reproduces the total charged particle multiplicity well, it consistently overpredicts the amount of fluctuations in multiplicity. When the jet production parameter in HIJING is turned off, the scaled variance as a function of centrality is independent of collision energy, illustrating that jet production accounts for the energy dependence of the HIJING results. Note that the HIJING results with jet production turned off are in better agreement with the data for all collision energies. Together with the observation that the multiplicity fluctuations demonstrate no significant p_T dependence, this may be an indication that correlated emission of particles from jet production do not significantly contribute to the multiplicity fluctuations observed in the data.

C. Comparisons to the clan model

The clan model [43] has been developed to interpret the fact that negative binomial distributions describe charged hadron multiplicity distributions in elementary and heavy ion collisions. In this model, hadron production is modeled as the independent emission of a number of hadronic clusters N_c, each with a mean number of hadrons n_c. The independent emission is described by a Poisson distribution with an average cluster, or clan, multiplicity of $\bar{N}_c$. After the clusters are emitted, they fragment into the final state hadrons. The measured value of the mean multiplicity μ_{ch} is related to the cluster multiplicities by $\mu_{\text{ch}} = \bar{N}_c \bar{n}_c$. In this model, the cluster multiplicity parameters can be simply related to the NBD parameters

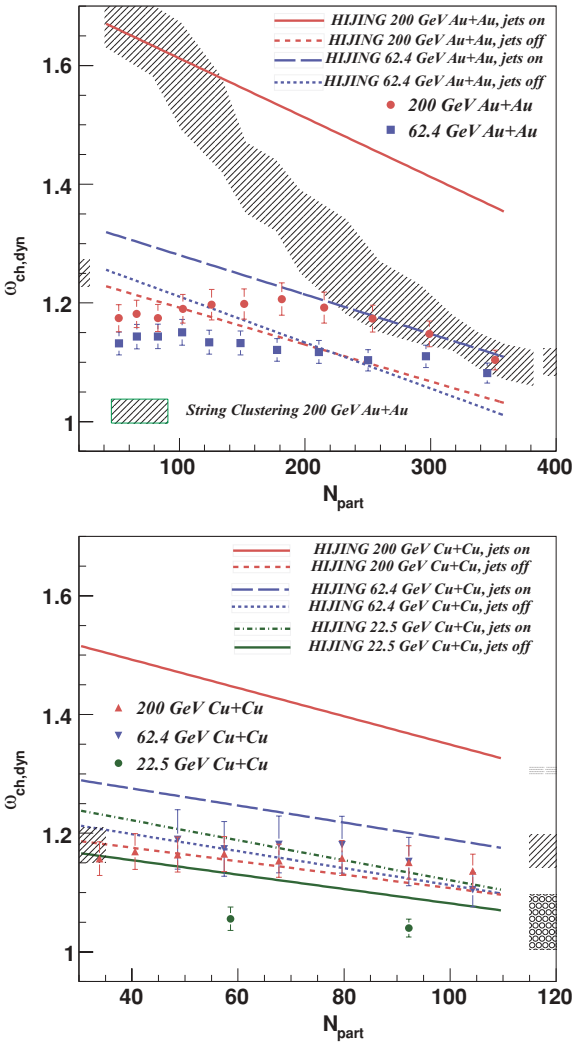

FIG. 11. (Color online) Fluctuations expressed as the scaled variance as a function of N_{part} for Au+Au and Cu+Cu collisions for $0.2 < p_T < 2.0$ GeV/c. The estimated contribution from geometry fluctuations has been removed. Results from the HIJING model code with jets turned on and jets turned off are overlaid with the shaded regions representing the systematic error for each curve.

of the measured multiplicity distribution as follows:

$$\bar{N}_c = k_{\text{NBD}} \ln(1 + \mu_{\text{ch}}/k_{\text{NBD}}), \tag{18}$$

and

$$\bar{n}_c = (\mu_{\text{ch}}/k_{\text{NBD}})/\ln(1 + \mu_{\text{ch}}/k_{\text{NBD}}). \tag{19}$$

The results from the NBD fits to the data are plotted in Fig. 12 for all collision species. Also shown are data from elementary and heavy ion collisions at various collision energies. The individual data points from all but the PHENIX data are taken from multiplicity distributions measured over varying ranges of pseudorapidity, while the PHENIX data are taken as a function of centrality. The characteristics of all of the heavy ion datasets are the same. The value of $\bar{n}_c$ varies little within the range 1.0–1.1. The heavy ion data universally exhibit only weak clustering characteristics as interpreted by the clan model. There is also no significant variation seen with collision energy. However, $\bar{n}_c$ is consistently significantly higher in elementary collisions. In elementary collisions, it is less probable to produce events with a high multiplicity, which can reveal rare sources of clusters such as jet production or multiple parton interactions.

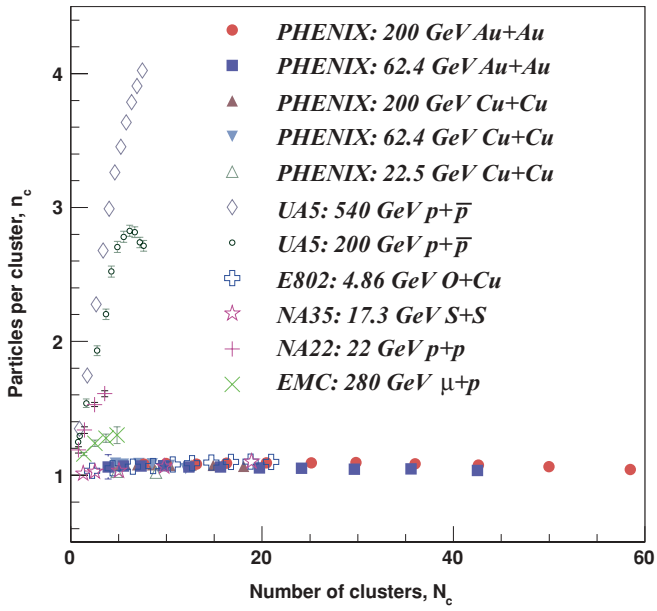

FIG. 12. (Color online) Correlation of the clan model parameters $\bar{n}_c$ and $\bar{N}_c$ for all collision species measured as a function of centrality. Also shown are results from pseudorapidity-dependent studies from elementary collisions (UA5 [17], EMC [18], and NA22 [19]) and heavy ion collisions (E802 [21] and NA35 [23]).

A feature that is especially apparent in the Au+Au data is the fact that the scaled variance decreases with increasing centrality, with the most central point lying below the participant superposition model expectation. The clan model provides one possible explanation for this effect whereby there is a higher probability for contributions from cluster sources such as jet production in the lower multiplicity peripheral events. The cluster sources introduce correlations that can increase the value of $1/k_{\text{NBD}}$ and hence the value of the scaled variance of the multiplicity distribution. Another possible explanation for this feature can be addressed with a string percolation model in heavy ion collisions [44]. In general, percolation theory considers the formation of clusters within a random spatial distribution of individual objects that are allowed to overlap with each other. The clusters are formed by the geometrical connection of one or more of the individual objects. This can be applied to estimate multiplicity fluctuations in heavy ion collisions whereby the objects are the circular cross sections of strings in the transverse plane [45] and the strings form clusters of overlapping strings that then each emit a number of particles related to the number of strings in each cluster. As the centrality increases, the number of individual clusters decreases along with the variance of the number of strings per cluster, which can result in a decrease in the magnitude of the resulting multiplicity fluctuations. The prediction of the scaled variance from the string percolation model for 200 GeV Au+Au collisions scaled down to the PHENIX acceptance in azimuth and pseudorapidity [45] is shown in

Fig. 11. Although percolation describes the trend observed at the four highest centralities very well, the scaled variance from the model continues to increase well above the data as centrality decreases. The implementation of the HIJING model contains merging of strings that are in close spatial proximity, so percolation can explain the trends in the scaled variance from HIJING.

An additional contribution to multiplicity fluctuations within the PHENIX acceptance arises from the presence of elliptic flow. This contribution has been estimated using a simple Monte Carlo simulation. In this simulation, a random reaction plane angle is assigned to each event. The multiplicity distribution due to the elliptic flow component is given by

$$dN/d\phi = C[1 + 2v_2 \cos(2\Delta\phi)], \tag{20}$$

where C is a normalization factor, v_2 is the measured magnitude of the elliptic flow, and $\Delta\phi$ is the difference between the particle emission angle and the reaction plane angle. For each event, this multiplicity distribution function is integrated over the PHENIX azimuthal acceptance and the resulting scaled variance from 1×10^6 events is calculated. The value of v_2 used in the simulation is taken from PHENIX measurements of elliptic flow at the mean transverse momentum of the inclusive charged hadron spectra [46,47]. The estimated contribution from elliptic flow to the observed scaled variance is shown in Fig. 5 for 200 and 62 GeV Au+Au collisions. This flow contribution also exhibits an increasing trend when moving from central to midcentral collisions. The estimated flow contribution increases from 18% of the signal in the most central 200 GeV Au+Au collisions to 35% of the signal at $N_{\text{part}} = 125$. In 62 GeV Au+Au collisions, the estimated flow contribution rises from 8% in the most central collisions to 25% at $N_{\text{part}} = 181$. The presence of elliptic flow can account for the majority of the centrality-dependent shapes observed in the Au+Au data.

VI. SUMMARY

PHENIX has completed a survey of multiplicity fluctuations of charged hadrons in Au+Au and Cu+Cu collisions at three collision energies. The motivation for the analysis is to search for signs of a phase transition or the presence of the predicted critical point on the QCD phase diagram by looking for increased multiplicity fluctuations as a function of system energy and system volume. After correcting for nondynamical fluctuations due to fluctuations of the collision geometry within a centrality bin, the multiplicity fluctuations in 200 and 62.4 GeV Au+Au collisions are consistent with or below the expectation from the superposition model of participant nucleons. The multiplicity fluctuations decrease as the collision centrality increases, dropping below the participant superposition model expectation for the most central Au+Au collisions. Fluctuations from Cu+Cu collisions exhibit a weaker centrality dependence that also is consistent with or below the expectation from the participant superposition model. The absence of large dynamical fluctuations in excess of the participant superposition model expectation indicate that there is no evidence of critical behavior related to the compressibility observable in this dataset. There is also no significant evidence of dynamical fluctuations that are dependent on the transverse momentum or the charge of the particles measured. As interpreted by the clan model, the observed fluctuations demonstrate only weak clustering characteristics for all of the heavy ion collision systems discussed here. The majority of the decreasing scaled variance with increasing centrality trend in Au+Au collisions can be explained by contributions from elliptic flow. Although this analysis does not observe evidence of critical behavior, it does not rule out the existence of a QCD critical point. Further measurements will be possible during the upcoming low-energy scan program at RHIC, allowing a more comprehensive search for critical behavior.

ACKNOWLEDGMENTS

We thank the staff of the Collider-Accelerator and Physics Departments at Brookhaven National Laboratory and the staff of the other PHENIX participating institutions for their vital contributions. We acknowledge support from the Office of Nuclear Physics in the Office of Science of the Department of Energy, the National Science Foundation, Abilene Christian University Research Council, Research Foundation of SUNY, and Dean of the College of Arts and Sciences, Vanderbilt University (U.S.A), Ministry of Education, Culture, Sports, Science, and Technology and the Japan Society for the Promotion of Science (Japan), Conselho Nacional de Desenvolvimento Científico e Tecnológico and Fundação de Amparo à Pesquisa do Estado de São Paulo (Brazil), Natural Science Foundation of China (People's Republic of China), Ministry of Education, Youth and Sports (Czech Republic), Centre National de la Recherche Scientifique, Commissariat à l'Énergie Atomique, and Institut National de Physique Nucléaire et de Physique des Particules (France), Ministry of Industry, Science and Tekhnologies, Bundesministerium für Bildung und Forschung, Deutscher Akademischer Austausch Dienst, and Alexander von Humboldt Stiftung (Germany), Hungarian National Science Fund, OTKA (Hungary), Department of Atomic Energy (India), Israel Science Foundation (Israel), Korea Research Foundation and Korea Science and Engineering Foundation (Korea), Ministry of Education and Science, Russia Academy of Sciences, Federal Agency of Atomic Energy (Russia), VR and the Wallenberg Foundation (Sweden), the US Civilian Research and Development Foundation for the Independent States of the Former Soviet Union, the US.-Hungarian NSF-OTKA-MTA, and the US-Israel Binational Science Foundation.

[1] M. A. Stephanov, K. Rajagopal, and E. V. Shuryak, Phys. Rev. Lett. **81**, 4816 (1998).

[2] M. A. Stephanov, in *LAT2006 Proceedings*, PoS(LAT2006)024 (SISSA, Trieste, Italy, 2006).

[3] K. Adcox *et al*. (PHENIX Collaboration), Nucl. Phys. **A757**, 184 (2005).
[4] S. Mrowczynski, Phys. Lett. **B430**, 9 (1998).
[5] V. V. Begun, M. I. Gorenstein, A. P. Kostyuk, and O. S. Zozulya, Phys. Rev. C **71**, 054904 (2005).
[6] S. Jeon and V. Koch, arXiv:hep-ph/0304012.
[7] V. V. Begun, M. Gazdzicki, M. I. Gorenstein, and O. S. Zozulya, Phys. Rev. C **70**, 034901 (2004).
[8] F. Becattini, A. Keranen, L. Ferroni, and T. Gabbriellini, Phys. Rev. C **72**, 064904 (2005).
[9] H. E. Stanley, *Introduction to Phase Transitions and Critical Phenomena* (Oxford University Press, New York, 1971).
[10] B. J. Schaefer and J. Wambach, Phys. Rev. D **75**, 085015 (2007).
[11] C. Sasaki, B. Friman, and K. Redlich, Phys. Rev. D **75**, 054026 (2007).
[12] I. N. Mishustin, Eur. Phys. J. A **30**, 311 (2006).
[13] M. A. Stephanov, K. Rajagopal, and E. V. Shuryak, Phys. Rev. D **60**, 114028 (1999).
[14] T. Kafka *et al*., Phys. Rev. Lett. **34**, 687 (1975).
[15] W. Thome *et al*. (Aachen-CERN-Heidelberg-Munich Collaboration), Nucl. Phys. **B129**, 365 (1977).
[16] G. J. Alner *et al*. (UA5 Collaboration), Phys. Lett. **B160**, 193 (1985).
[17] G. J. Alner *et al*. (UA5 Collaboration), Phys. Rep. **154**, 247 (1987).
[18] M. Arneodo *et al*. (European Muon Collaboration), Z. Phys. C **35**, 335 (1987) [Erratum-*ibid*. **36**, 512 (1987)].
[19] M. Adamus *et al*. (EHS/NA22 Collaboration), Z. Phys. C **37**, 215 (1988).
[20] R. E. Ansorge *et al*. (UA5 Collaboration), Z. Phys. C **43**, 357 (1989).
[21] T. Abbott *et al*. (E-802 Collaboration), Phys. Rev. C **52**, 2663 (1995).
[22] R. Albrecht *et al*. (WA80 Collaboration), Z. Phys. C **45**, 31 (1989).
[23] J. Bachler *et al*. (NA35 Collaboration), Z. Phys. C **57**, 541 (1993).
[24] M. M. Aggarwal *et al*. (WA98 Collaboration), Phys. Rev. C **65**, 054912 (2002).
[25] C. Alt *et al*. (NA49 Collaboration), Phys. Rev. C **75**, 064904 (2007).
[26] S. S. Adler *et al*. (PHENIX Collaboration), Phys. Rev. C **76**, 034903 (2007).
[27] K. Adcox *et al*. (PHENIX Collaboration), Nucl. Instrum. Methods Phys. Res. A **499**, 469 (2003).
[28] K. Adcox *et al*. (PHENIX Collaboration), Nucl. Instrum. Methods Phys. Res. A **499**, 489 (2003).
[29] M. Aizawa *et al*. (PHENIX Collaboration), Nucl. Instrum. Methods Phys. Res. A **499**, 508 (2003).
[30] L. Aphecetche *et al*. (PHENIX Collaboration), Nucl. Instrum. Methods Phys. Res. A **499**, 521 (2003).
[31] J. T. Mitchell *et al*. (PHENIX Collaboration), Nucl. Instrum. Methods Phys. Res. A **482**, 491 (2002).
[32] M. Allen *et al*. (PHENIX Collaboration), Nucl. Instrum. Methods Phys. Res. A **499**, 549 (2003).
[33] S. S. Adler *et al*. (PHENIX Collaboration), Phys. Rev. C **71**, 034908 (2005); **71**, 049901(E) (2005).
[34] M. L. Miller, K. Reygers, S. J. Sanders, and P. Steinberg, Annu. Rev. Nucl. Part. Sci. **57**, 205 (2007).
[35] H. Heiselberg, Phys. Rep. **351**, 161 (2001).
[36] S. S. Adler *et al*. (PHENIX Collaboration), Phys. Rev. C **69**, 034909 (2004).
[37] V. P. Konchakovski, M. I. Gorenstein, E. L. Bratkovskaya, and H. Stocker, Phys. Rev. C **74**, 064911 (2006).
[38] B. Lungwitz and M. Bleicher, Phys. Rev. C **76**, 044904 (2007).
[39] V. P. Konchakovski, M. I. Gorenstein, and E. L. Bratkovskaya, Phys. Rev. C **76**, 031901(R) (2007).
[40] V. P. Konchakovski, S. Haussler, M. I. Gorenstein, E. L. Bratkovskaya, M. Bleicher, and H. Stocker, Phys. Rev. C **73**, 034902 (2006).
[41] X. N. Wang and M. Gyulassy, Phys. Rev. D **44**, 3501 (1991).
[42] A. Bialas, M. Bleszynski, and W. Czyz, Nucl. Phys. **B111**, 461 (1976).
[43] A. Giovannini and L. Van Hove, Z. Phys. C **30**, 391 (1986).
[44] M. Nardi and H. Satz, Phys. Lett. **B442**, 14 (1998).
[45] L. Cunqueiro, E. G. Ferreiro, F. del Moral, and C. Pajares, Phys. Rev. C **72**, 024907 (2005).
[46] S. S. Adler *et al*. (PHENIX Collaboration), Phys. Rev. Lett. **94**, 232302 (2005).
[47] A. Adare *et al*. (PHENIX Collaboration), Phys. Rev. Lett. **98**, 162301 (2007).